ACS OMEGA

http://pubs.acs.org/journal/acsodf

Article

Extraction of Humic Acids from Lignite and Its Use as a Biochar Activator

Huijin Li, Shuang Ding, and Jie Yuan*

Cite This: *ACS Omega* 2023, 8, 12206−12216

Read Online

ACCESS | Metrics & More | Article Recommendations

ABSTRACT: Current research focuses on extracting humic acid (HA) compounds from low-rank coals to obtain high value-added products. In this study, HAs with high purity and low heavy metal content were obtained from lignite by combining acid pretreatment with hydrothermal treatment. Scanning electron microscopy, elemental analysis (EA), Fourier transform infrared (FTIR) spectroscopy, X-ray diffraction, and inductively coupled plasma optical emission spectrometry (ICP−OES) were used to analyze raw lignite and HAs. The effects of acid and hydrothermal treatments on the inorganic elements, functional groups, and yield of HAs were examined. The results showed that acid treatment reduced the ash content of lignite from 20 to 9%, and hydrothermal treatment increased the yield of HAs from 36 to 68%. The chemical properties of HAs exhibited an increase in molecular weight and improved aromaticity after acid and hydrothermal treatments. The results of ICP−OES analysis suggested that the combined method of acid and hydrothermal treatments resulted in a significant reduction of heavy metal elements in HAs. FTIR analysis confirmed the results and demonstrated that the extracted HA from nitric acid pretreated and hydrothermal generation of lignite PHA was rich in carboxyl and phenolic functional groups. PHA was applied to biochar as an activator for the adsorption of heavy metal ions. The experimental results showed that PHA was successfully loaded onto biochar and introduced a large number of functional groups, and the adsorption capacity of the modified biochar for Pb^{2+} was effectively improved.

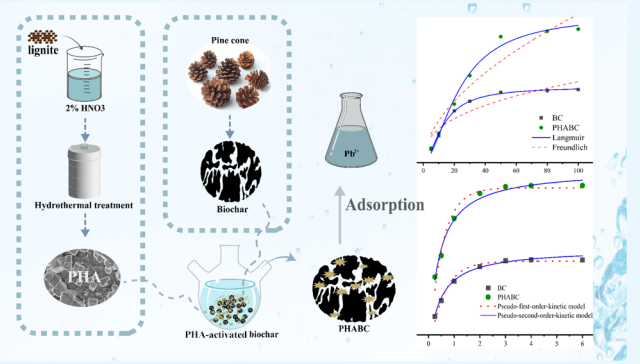

1. INTRODUCTION

Humic acids (HAs) are high-molecular-weight biopolymers that can usually be generated from organic matter humic compounds in soils, peat and humus, natural water bodies, and low-rank coals.[1,2] They are soluble in alkaline media, partially soluble in water, and insoluble in acidic media fractions.[3] HAs contain different functional groups, mainly including phenolic, carboxylic, quinone, and ether functional groups, and probably including sugars and peptides.[4] Therefore, the chemical structure of humic substances is a random polycondensation with a conjugated aromatic backbone.[5,6] Phenolic and carboxyl groups are more prevalent in the HA structure, explaining the acidity of HAs.

Studies show that oil, coal, and natural gas contribute about 85% of the world's total energy consumption.[7] There is a growing interest in developing sustainable technological processes based on renewable bio-based materials, and economically viable production processes for the synthesis of chemical intermediates from biomass carbohydrates are seen as a major challenge.[8,9] Currently, extracting humic substances from low-rank coals to obtain higher value-added products is the focus of research by a variety of industrial and academic research groups.[10] In general, HA production is based on the reaction of medium acidic oxygen-containing functional groups of coal with alkaline reagents to produce soluble humates, followed by the precipitation of soluble humates with acidic reagents and finally the filtration or centrifugation of the sediment.[10] Zara et al.[11] extracted HAs from Pakistani lignite by nitric acid (HNO_3) oxidation and potassium hydroxide (KOH) solubilization. Stefanova et al.[12] extracted HAs from Bulgarian lignite. The conventional alkali solubilization and acid precipitation method using sodium hydroxide (NaOH) dissolution and hydrochloric acid (HCl) precipitation obtained 83% of HA content, which is simple to operate, but the extracted HAs have low-purity and high-content heavy metal elements. Lignite is an ideal raw material and a typical low-rank coal, accounting for about 45% of coal reserves in the world.[13] HAs extracted from lignite have abundant aromatic groups, high carbon content and biochem-

Received: December 26, 2022
Accepted: March 16, 2023
Published: March 24, 2023

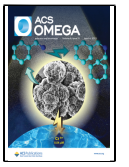

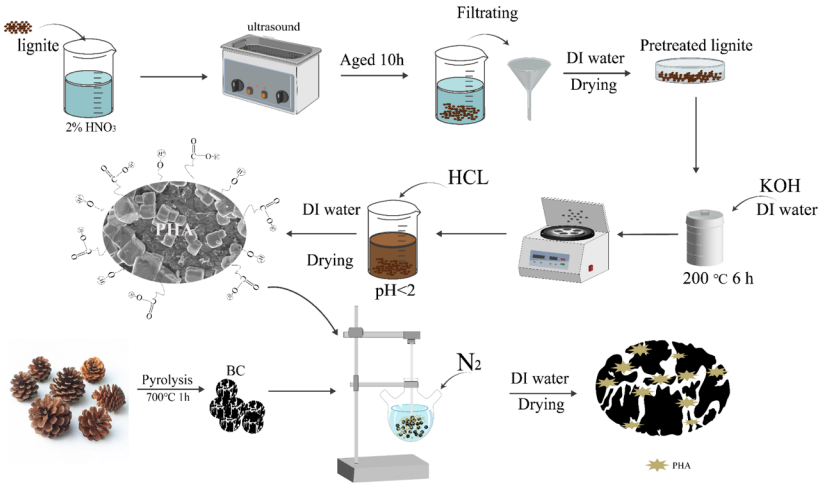

Figure 1. Preparation process for PHA and PHABC.

ical activity, low oxygen and nitrogen content, as well as methylene and ethylene bridges between aromatic rings.[14]

Lignite comprises a large number of mineral components, of which the most common minerals are kaolinite, pyrite, calcite, montmorillonite, and rhodochrosite.[15] Usually, the content of mineral components is proportional to that of ash, which is a quantitative measure of inorganic impurities in HAs. Some studies have reported that the ash content in extracted HA and fulvic acid structures exceeds 5%.[16] Reducing the ash content and improving the purity of HAs are of interest in a vast array of applications. Acid pretreatment removes minerals from coal, increases its pore structure and oxygen-containing functional groups, and changes its hydrogen/carbon (H/C) ratio.[17] Jaiswal et al.[18] found that HNO_3 could remove organic sulfur (up to 53.96%) from lignite samples. Huang et al.[19] used HNO_3-modified lignite to enhance the adsorption capacity of lignite for Pb^{2+}. HNO_3 interacted with the iron dolomite in lignite and inorganic mineral impurities, like organic components in lignite, which decreased the specific surface area and increased the pore size and the content of polar oxygen-containing functional groups, such as hydroxyl, carbonyl, and carboxyl groups, on the lignite surface.

Based on the theory that subcritical water can dissolve organic matter, hydrothermal extraction refers to the hydrothermal condensation of biomass under the conditions of oxygen exclusion and autogenous pressure in a special closed vessel.[20] Hydrothermal treatment facilitates the dissociation of the aggregated structures (pore and mineral structures) of coal, thus increasing the separation efficiency.[21] Liu et al.[22] studied the hydrothermal removal of oxygen functional groups from lignite and noticed that the contents of carboxyl, alcohol hydroxyl, ether, and carbonyl groups decreased with the increase of temperature after the hydrothermal treatment of lignite samples, while that of phenolic hydroxyl groups remained essentially unchanged. As concluded by Yang and Antonietti,[3] hydrothermal humification can be regarded as a mild chemical engineering process mimicking natural decay. They directly compared the HAs extracted by hydrothermal extraction with the natural humic substances extracted from the black soil of Harbin, China, and noted that the chemical structures and elemental contents of both HAs were highly similar.

A review by Tang et al.[23] reported that HAs can interact with nanomaterials in complexes with metal ions and exert an impact on the removal and migration of heavy metals by nanomaterials. The ability of HAs to bind heavy metals can be used to carry out research on remediation techniques for heavy metals in wastewater. Several studies[24−27] have also previously applied HA to activated biochar. This is also environmentally friendly because the residual HA after activation of biochar can be simply recovered by hydrochloric acid decomposition. Biochar is a low-cost and efficient adsorption material with a wide range of applications in the removal of heavy metals,[28] which, however, has limited adsorption capacity and whose performance is generally improved by a modification to strengthen adsorption capacity and stability.[29] Thus, in this study, HAs were extracted by hydrothermal alkaline leaching after the selection of the HNO_3 pretreatment of low-rank lignite and used for biochar modification to obtain modified biochar with excellent adsorption performance for heavy metal ions.

2. MATERIALS AND METHODS

2.1. Reagents. Pine cones were bought locally, crushed to a size of 1−2 cm, cleaned, and dried before use. The lignite used for experiments was obtained from Zhaotong, Yunnan Province, China. Reagents KOH, concentrated HNO_3, concentrated HCl, ammonia monohydrate (NH_3H_2O), NaOH, and lead nitrate $Pb(NO_3)_2$ were purchased from the Aladdin website. Deionized water (DI) was generated by the use of a Milli-Q water purification system. All compounds were used as received.

2.2. Experimental Section. *2.2.1. Lignite Pretreatment.* Lignite was crushed and sieved through a 60 mesh sieve and dried in a vacuum oven at 105 °C to a constant weight. In this paper, ultrasound-assisted acid pretreatment of lignite was used. 20 g of lignite was taken, added to 100 mL of a 2% HNO_3 solution in a beaker, mixed ultrasonically for 2 h, and then left for 10 h. Then, it was filtered and washed repeatedly with DI until it was about neutral and dried at 40 °C in an oven.

2.2.2. HA Extraction. Acid pretreatment combined with hydrothermal: the pretreated lignite (3 g), KOH (3 g), and DI (60 mL) in a hydrothermal reactor were held in an oven at 200 °C for 6 h. After cooling to room temperature, the supernatant and residue were separated by centrifugation, of which the latter was washed repeatedly with DI to neutral. The supernatant and the residue washing solution were acidified with hydrochloric acid at pH < 2, centrifuged and filtered after standing for obvious stratification, and dried at 60 °C in a vacuum drying oven to get HAs named PHA.

https://doi.org/10.1021/acsomega.2c08192
ACS Omega 2023, 8, 12206−12216

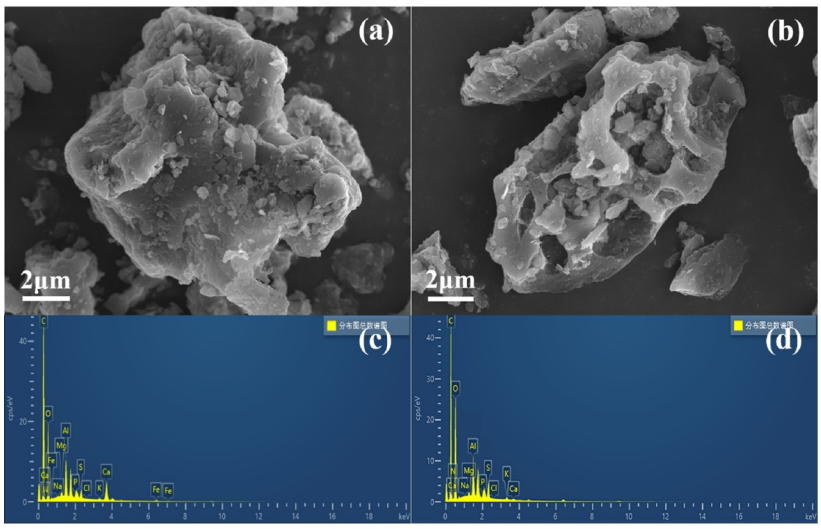

Figure 2. SEM and EDS scan: (a,c) lignite and (b,d) HNO_3-pretreated lignite.

2.2.2.1. Hydrothermal. To test the effect of lignite pretreatment on the extraction of HAs, the same experimental procedure was used for obtaining HAs from lignite, named HA.

2.2.2.2. Acid Pretreatment. The effect of the hydrothermal method on HA extraction was studied by comparing it with the commonly used alkali-soluble acid precipitation method. The pretreated lignite and KOH were taken at 3 g, respectively, mixed with 60 mL of DI in a 250 mL beaker, stirred well and left for 12 h. The remaining steps were the same as those of the hydrothermal method, named NHA.

The HA yield was calculated on an air-dried basis according to the following equation

$$\text{yield}\ (\%) = \frac{M_Y(1 - M_{ad}) - M_C}{M_Y(1 - M_{ad})} \times 100\% \quad (1)$$

where M_Y (g) represents the mass of lignite; M_{ad} (%) stands for the water content in the raw lignite; M_C (g) denotes the mass of the residue remaining after HA extraction. The moisture content (M_{ad}) and ash content (A_{ad}) tests of the samples were performed on the basis of the standard GB/T212-2008.[30]

2.2.3. PHA-Activated Biochar. The method of biochar activation by HAs was referred to Du et al.[31] Pine cones were crushed and passed through a 100 mesh sieve. The crushed and dried pine cone powder was heated to 700 °C at 5 °C·min^{-1} in a tube furnace and held for 1 h to obtain biochar (BC). Next, 1 g of BC and 50 mL of DI were added to a three-neck flask and stirred at 150 rpm for 15 min to fully disperse the biochar powder in the water, followed by the dissolution of PHA (50 mg) in 20 mL of a 6% ammonia solution. After complete dissolution, it was added to a three-neck flask and continuously stirred at 150 rpm for 3 h in a nitrogen-rich environment. The precipitate was separated by filtration, washed several times, and dried at 70 °C in an oven to obtain PHA-modified BC (PHABC).

The preparation process of all materials is shown in Figure 1.

2.2.4. Adsorption Experiment of Heavy Metal Ions. The adsorption experiments were carried out in 100 mL conical flasks containing 40 mL of the solution in a constant temperature oscillator. The effects of pH (2−10) and adsorbent dosing (5−100 mg) on Pb^{2+} adsorption were investigated. The pH was adjusted with HNO_3 or NaOH (0.1 M), and all experiments were carried out at room temperature (25 ± 1 °C). Kinetic experiments were completed at an adsorbent dosing of 10 mg, Pb^{2+} concentration of 50 mg/L, pH of 7 (±0.2), and predetermined time intervals (0.25, 1, 2, 3, 4, and 6 h). For the thermodynamic experiments, the contact time for Pb^{2+} was 2 h. The addition of solutions with different initial concentrations of heavy metal ions (5−100 mg) was done under the homogeneous conditions described above for the adsorption kinetics experiments. Then, the lead-loaded samples were separated by filtration, and the residual supernatant Pb^{2+} concentration was evaluated with ICE-3500 to obtain the Pb^{2+} removal capacity. The adsorption volume (Qe) was calculated according to eq 2.

$$\text{Qe} = \frac{(C_0 - C_e)V}{m} \quad (2)$$

where Qe represents the amount of Pb^{2+} adsorbed at moment t (mg/g); m stands for the weight of BC (g); V denotes the solution volume (L); C_0 and C_e refer to the solution concentrations of Pb^{2+} initially and at moment, respectively.

The dynamics and kinetics of Pb^{2+} adsorption on BC were simulated by use of the pseudo-first-order (PFO) and pseudo-second-order (PSO) kinetic models (eqs 3 and 4).

$$q_t = \frac{q_e(e^{-tk_1} - 1)}{e^{-tk_1}} \quad (3)$$

$$q_t = \frac{q_e t}{\left(t + \frac{1}{k_2 q_e}\right)} \quad (4)$$

where q_e (mg/g) represents the removal rate at equilibrium; q_t (mg/g) stands for the instantaneous removal rate (h); k_1 (h^{-1}) and k_2 [g/(mg·h)] refer to the rate constants of PFO and PSO adsorption kinetic models, respectively.

The adsorption isotherm data of Pb^{2+} were fitted using Langmuir (LM, eq 5) and Freundlich (FM, eq 6) models.

$$q_e = \frac{q_m K_L C_e}{1 + K_L C_e} \quad (5)$$

$$q_e = K_F C_e^{1/n} \quad (6)$$

where C_e and q_e represent the equilibrium water concentration and adsorption capacity of Pb^{2+} (mg/L and mg/g), respectively.

https://doi.org/10.1021/acsomega.2c08192
ACS Omega 2023, 8, 12206−12216

Table 1. Surface Element Composition of Lignite and HNO_3-Pretreated Lignite

	element (weight composition %)										
samples	C	O	Na	Mg	Al	P	S	Cl	K	Ca	Fe
lignite	63.03	27.01	0.02	0.58	3.05	0.41	0.97		0.20	3.56	0.76
HNO_3-pretreated lignite	62.32	33.12	0.01	0.24	2.89	0.30	0.54	0.01	0.01	0.01	

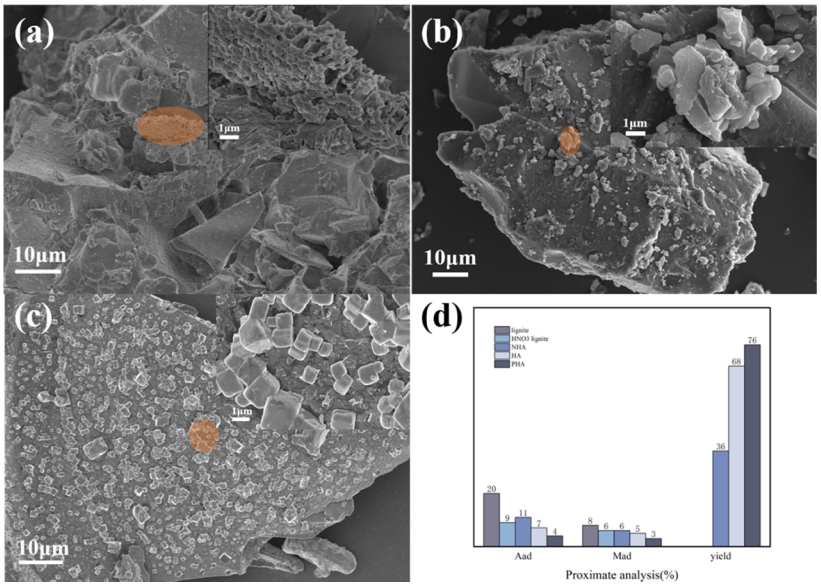

Figure 3. SEM image of HA: (a) NHA; (b) HA; (c) PHA; (d) industrial analysis and production of lignite samples and HAs.

Parameters K_F and K_L stand for the adsorption coefficients of FM and LM [$(mg/g)(mg/L)^{-n}$ and L/mg], respectively. Besides, q_m denotes the maximum adsorptive power of the solute (mg/g), and n refers to the Freundlich constant indicating the nonlinearity degree.

2.3. Characterizations. The elemental composition of lignite samples and HAs was measured using an elemental analyzer (Vario MICRO cube, Germany). Absorption ratios were determined by ultraviolet−visible (UV−vis) spectrophotometry with a UV−vis spectrophotometer (PERSEE TU-1901, China). The morphology and elemental composition of materials were characterized by scanning electron microscopy (SEM, TESCAN MIRA LMS, Czech Republic) in combination with energy dispersive X-ray spectroscopy (EDS). The Fourier transform infrared (FTIR) spectra of the samples in the range of 4000−400 cm^{-1} were examined using an FTIR spectrometer (Thermo Scientific Nicolet 6700, the United States of America (USA)). X-ray diffraction (XRD) analysis was conducted on an X-ray diffractometer equipped with a Cu Kα X-ray radiation source and a Bragg diffraction unit (Shimadzu 7000S). Nitrogen adsorption and desorption tests were performed with a fully automated specific surface and porosity analyzer (Micromeritics ASAP 2460, USA) to determine the surface area and pore size distribution. Inductively coupled plasma mass spectrometry (ICP−MS, Thermo Fisher iCAP PRO (OES), USA) was used to measure the inorganic element content in the raw lignite and PHA. The remaining Pb^{2+} concentration in the solution was measured using an atomic absorption spectrometer (Thermo Fisher ICE-3500, USA) in the biochar adsorption experiment.

3. RESULTS AND DISCUSSION

3.1. Raw Material Analysis. The surface morphology of the samples is presented in Figure 2. Lignite (Figure 2a) has a smooth surface without obvious openings. In contrast, the HNO_3-treated lignite (Figure 2b) indicates a broken and irregular structure with larger pores. Acid treatment promoted the evolution of internal pores and the enlargement of pore size of lignite and lifted the number of internal mesopores and macropores of lignite. This is due to the acid treatment removed mineral particles, like kaolinite and calcite, attached to the lignite surface, which changed the surface morphology and pore size of lignite. The EDS energy spectrum in Figure 2c,d also listed the elemental distribution on the surface of lignite and HNO_3-pretreated lignite. As illustrated in Table 1, the lignite treated with HNO_3 was dominated by the addition of oxygen and reduction of mineral elements, indicating that acid treatment effectively removed ash and mineral components from lignite. This was further confirmed by the ash analysis in Figure 3d, where the ash content in the original lignite was as high as 20% and reduced to 9% after acid treatment.

3.2. Analysis and Characterization of HAs. *3.2.1. Micromorphology and Elemental Composition.* The extracted HAs were analyzed by SEM in Figure 3a−c. NHA has a rough and irregular surface, with obvious pores between structures. Hydrothermal treatment contributed to the smooth and nonporous surfaces of HA and PHA. Compared with HA, PHA particles were more uniform in size, cubic in shape, and uniformly distributed on the surface with a particle size of 1−2 μm.

The elemental analysis (EA) results of lignite samples NHA, HA, and PHA before and after HNO_3 pretreatment are summarized in Table 2. Compared with the raw lignite, carbon content decreased after HNO_3 treatment, indicating the effectiveness of acid treatment in decarburization. The increase in the oxygen content was attributed to the oxidation process of HNO_3, leading to the addition of more oxygen-containing

https://doi.org/10.1021/acsomega.2c08192
ACS Omega 2023, 8, 12206−12216

Table 2. Elemental Composition

samples	ultimate analysis (%)			atomic ratios		
	C	H	O[a]	N	O/C	H/C
lignite	69.01	4.71	24.06	1.91	0.349	0.068
HNO_3-pretreated lignite	65.58	4.71	27.33	2.13	0.416	0.072
NHA	57.53	4.54	22.86	2.23	0.397	0.078
HA	55.37	5.02	25.88	2.73	0.467	0.091
PHA	56.89	4.78	23.13	2.90	0.406	0.084

[a]Represents the value obtained using the difference subtraction method.

functional groups. Wang et al.[32] investigated the oxidation characteristics of lignite by acid treatment and obtained the following findings: The X-ray photoelectron spectroscopy (XPS) structure showed a decrease in carbon−carbon/carbon−hydrogen (C−C/C−H) content and a significant increase in relative carbon-oxygen (C−O) content after HNO_3 treatment from 5.49 to 9.23% of the original lignite, and the alkane C−H in lignite was gradually oxidized and converted to C−O or C═O bands, thereby increasing the content of oxygen-containing groups in lignite. This is consistent with the analytical results of EDS (Table 1). Nitrogen content also experienced an increase through the nitrification reaction of lignite during the oxidation of acid pretreatment, which introduced nitrate as a functional group. O/C and H/C atomic ratios were used as indicators for the determination of aromaticity, and aromaticity was lower when O/C and H/C atomic ratios were higher. It can be seen from the table that the hydrothermal treatment decreased the aromaticity of HAs, which, however, was increased by acid treatment.

As shown in Figure 3d, both acid and hydrothermal treatments were effective in ash removal, and the simultaneous use of both methods reduced the ash content of PHA from 20 to 4% in the original lignite. Hydrothermal treatment increased the HA yield from 36 to 68%, and hydrothermal heat resulted in a great increase in HA yield. On this basis, the pretreatment of lignite samples again increased the HA yield from 68 to 76%, revealing that the combination of acid treatment and hydrothermal heat is an effective method of extracting HAs.

3.2.2. Aromaticity and Functional Groups of HAs. As an important indicator for the structural characterization of HA composition, E4/E6 indicates the optical density ratio of the measured solution at wavelengths 465 and 665 nm.[33] Reflecting relative molecular mass or the degree of aromatic condensation of HAs, the ratio usually has a negative relationship with molecular mass or the degree of condensation. HA of 5 mg was dissolved in 100 mL of 0.05 M $NaHCO_3$ solution (pH 8.4) and centrifuged at 7000 rpm at room temperature for 5 min. Sodium bicarbonate buffer was used as a blank, and absorbance values were obtained at the wavelengths 465 and 665 nm.

In the present study, the maximum E4/E6 ratio was 2.92 for HA, and 2.28 for PHA, as shown in Table 3. Acid treatment increased the molecular weight and aromatic content of HAs,

Table 3. E4/E6 Ratio of Humic Acids

samples	E4	E6	E4/E6
NHA	0.134	0.060	2.23
HA	0.076	0.026	2.92
PHA	0.043	0.019	2.28

also demonstrating an increase in the biological activity of molecules. This was also observed by the EA presented in Table 2. In contrast, the study by Fatima et al.[34] showed that the aromatization of HAs decreased after acid treatment.

With a complex composition and structure, HAs contain various functional groups, such as hydroxyl (alcohols and phenols), carboxyl (aliphatic and aromatic hydrocarbons), and ketone groups (quinone and ketone types). By comparing the FTIR of the three samples in Figure 4, some co-existing

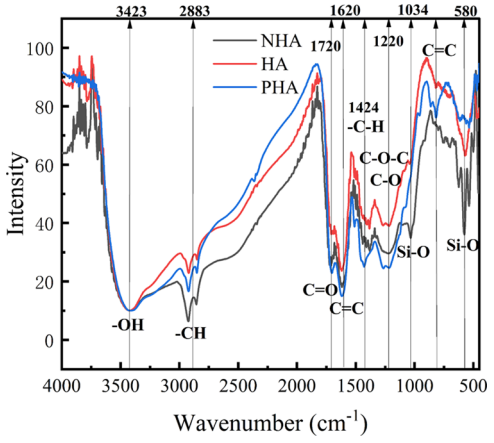

Figure 4. Infrared spectra of the extracted HAs.

characteristic peaks can be seen, and the effects of different treatments on the functional groups of HAs can be judged from the change of peak intensity and the appearance of peaks.

A strong and broad absorption peak appeared in the range of 3300−3600 cm^{-1}, which should be the telescopic vibration peak of −OH of phenols and carboxyl groups, etc., since lignite contains almost no alcohol functional groups. The intensity of the peak showed no significant changes, indicating that hydrothermal and acid pretreatments had little effect on the total content of hydroxyl groups. Characteristic peaks located at 2925 and 2852 cm^{-1} belonged to the fatty structures of −C−H, $-CH_2$, and CH_3 stretching vibrations, with HA and PHA showing reduced peak intensities relative to NHA, signifying that both hydrothermal and acid treatments reduced fatty carbon chains; this is consistent with previous studies.[35] A strong C═O stretching vibration peak of the carboxyl group appeared at 1720 cm^{-1}. The strong absorption of C═O vibrations at 1714 cm^{-1} by HAs has been suggested by Gómez-Serrano et al.[36] as the most characteristic spectral feature of HAs abundant in low-rank coals. The characteristic peak at 1620 cm^{-1} was the absorption peak C═C of an aromatic conjugated double bond, an indicator of the aromaticity and condensation of molecules. The intensity of the peak was slightly reduced in HA relative to NHA, while that of PHA was slightly enhanced here, indicating that hydrothermal treatment may have reduced the number of aromatics and acid pretreatment increased the polymer of HAs. The characteristic peak at 1424 cm^{-1} was the −C−H bending vibration of the aliphatic structure, which was basically absent for NHA and HA. The obvious peak appeared for PHA. The characteristic peak at 1387 cm^{-1} was the C−H deformation vibration peak of C−O stretching, $-CH_2$ and CH_3, which was presumed to be probably $-CH_2$ and CH_3 changed relatively little during hydrothermal treatment, but methyl and methylene groups were substituted or oxidized during acid pretreatment, forming more −CH. At 1220 and 1266 cm^{-1} are C−O and C−

https://doi.org/10.1021/acsomega.2c08192
ACS Omega 2023, 8, 12206−12216

O−C stretching vibrational peaks of esters, alcohols, carbohydrates, and aryl groups. PHA was enhanced compared with NHA, indicating that acid treatment favored the formation of C−O and C−O−C. The peak at 1034 cm^{-1} is probably Si−O of silica impurities with strong NHA and disappearance of HA and PHA, which should have been removed by dissolution during acid pretreatment and hydrothermal treatment. XRD in Figure 5

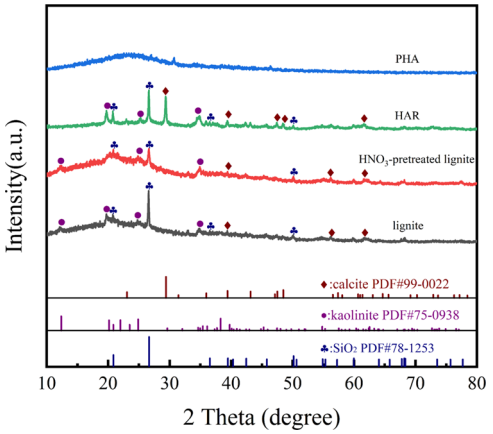

Figure 5. XRD patterns of samples, HNO_3-pretreated lignite, HA residue extraction (HAR), and PHA.

also showed that the original lignite contains more mineral components, which were greatly reduced after acid treatment. Characteristic peaks in PHA hardly appeared after the hydrothermal treatment. While the peak at 814 cm^{-1} was the peak of the aromatic ring, the variation pattern was consistent with that of the peak at 1620 cm^{-1}, which was significantly enhanced after acid treatment. Consistent with previous studies,[37] peaks at 580 and 623 cm^{-1} were presumed to be those of inorganic oxides, which may be the stretching vibration of Si−O, and were reduced after hydrothermal treatment.

3.2.3. Inorganic Elements and Mineral Components. As presented in Figure 5, the main mineral components in experimental lignite are silica, kaolinite, and calcite. Low pH facilitates the dissolution of metal ions. The characteristic peaks of these minerals gradually disappeared after HNO_3 treatment. In other words, minerals were removed. The EDS spectrum analysis in Figure 2 also shows that the lignite surface contains more and mineral elements than HNO3-pretreated lignite. The diffraction peaks of silicon dioxide (SiO_2) and calcite crystal faces in the HA residue were very sharp compared with those of the HNO_3-treated lignite. This difference was ascribed to the fact that hydrothermal treatment destroyed the chelation of HAs with metallic elements, effectively reducing their content. Shi et al.[38] described that hydrothermal treatment broke the weaker covalent bonds of ethers and esters and changed the distribution of hydrogen bonds in coal. Thus, reducing the content of inorganic elements in HAs. Subcritical water has the characteristics of enhanced self-ionization and reduced viscosity and surface tension, which make it have an acid−base catalytic function and facilitate the contact of reactants and hydrolysis of organic macromolecules, thus reducing the mass transfer resistance and increasing the reaction rate.[39,40] Moreover, the addition of HCl during the acidification process also ionizes the hydroxide precipitation produced by the reaction with KOH, thus reducing the content of inorganic elements in HAs.

The analysis of the samples by inductively coupled plasma optical emission spectrometer (ICP−OES) was performed to evaluate the contents of heavy metals and inorganic impurities in PHA. Inorganic elements, such as dangerous chemicals and toxic substances, including heavy metals, should be kept at low concentrations in HAs. As shown in Table 4, the highest concentration of K (13,139.3 ppm) was found in the produced HAs, which may be due to the alkaline extraction of humic compounds from lignite using KOH. The content of S (1971 ppm), Fe (559 ppm), and Al (1150 ppm) was also relatively high, which was related to the material nature of lignite itself. The content of the remaining elements was very low, less than 100 ppm. Kurková et al.[41] analyzed the elemental content of extracted HAs, including Cd [0.2 parts per million (ppm)], As (4.5 ppm), Pb (5.7 ppm), Zn (4.2 ppm), Cu (22.2 ppm), V (11.4 ppm), Ni (17.5 ppm), Cr (26.1 ppm), and Al (749 ppm). Compared with them, the heavy metal content of HAs extracted in this study was much lower.

3.3. Experiment of PHA-Modified Biochar Adsorption of Lead Ions. *3.3.1. Biochar Properties.* The surface of pine cone biochar in Figure 6b was uniformly distributed with agglomerated aggregates. Compared with the surface of pine cone biochar in Figure 6b, that in Figure 6a was smooth with the presence of more porosity, indicating that PHA was successfully loaded onto BC. Nevertheless, some pores on the surface of HAs were blocked because of HA loading, and the increase in surface compactness led to a decreased specific surface area of biochar, which is also in line with the results in Table 5. After the addition of PHA, the specific surface area Brunauer−Emmett−Teller (SBET) of BC dropped from 443.96 to 247.67 $m^2 \cdot g^{-1}$, and pore volume gradually rose from 0.013 to 0.132 $cm^3 \cdot g^{-1}$. However, the decrease in the specific surface area does not imply a decrease in adsorption capacity. The chemical properties of biochar have been observed to be more important than the surface area in heavy metal adsorption.[42] Imran et al.[43] prepared complexes of quinoa biochar with magnetite nanoparticles. Despite the reduction in the surface area, the adsorption capacity of the modified biochar was enhanced approximately twofold compared with that of the pristine biochar.

Table 4. Concentrations (ppm) of Inorganic Elements and Heavy Metals in Lignite and PHA in This Study

element	Cu	Zn	Fe	Cr	P	Al	Si	As
lignite	20.1	19.3	10663.9	47.1	321.3	24659.8	744.3	155.3
PHA	<0.1	1.4	558.9	<0.1	37.6	1150.4	17.8	5.3
element	Ni	Mo	Mn	Pb	Cd	V	Ti	Zr
lignite	33.2	1.23	111.1	4.5	0.4	16.8	2132.8	45.5
PHA	0.9	0.6	3.2	<0.05	<0.1	<0.01	89.9	13.9
element	Sr	Ba	K	Ca	Na	Mg	S	Li
lignite	185.6	111.1	907.4	3136.8	33.2	837.3	11245.9	8.2
PHA	9.4	15.2	13139.3	21.7	19.3	18.3	1971.3	<0.1

https://doi.org/10.1021/acsomega.2c08192
ACS Omega 2023, 8, 12206−12216

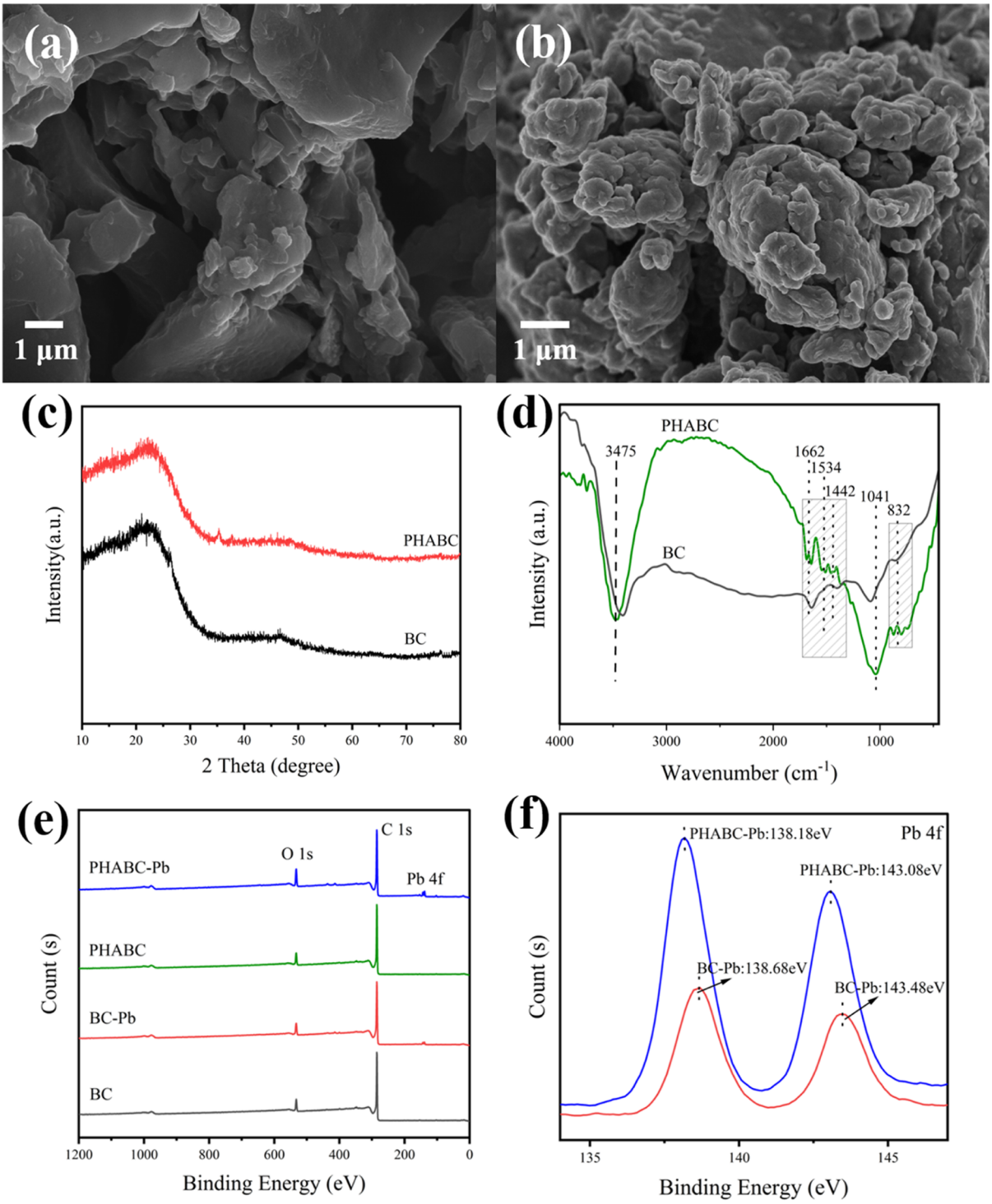

Figure 6. SEM images: (a) BC; (b) PHABC; (c) XRD patterns of BCs; (d) FTIR patterns of BCs; (e) wide-scan spectrum of BCs before and after sorption of Pb^{2+}; (f) Pb 4f.

Table 5. Pore Structure Data for BC and PHABC

	BET	BJH desorption	
materials	surface area (m^2/g)	cumulative volume of pores (cm^3/g)	average pore diameter (nm)
BC	443.96	0.013	3.12
PHABC	247.67	0.132	10.45

XRD (Figure 6c) showed no significant characteristic peaks of the pine cone char after HA introduction, demonstrating that the structure of the pine cone char remained stable after HA modification. After the introduction of PHA, the functional groups of biochar went through significant changes. It can be seen from Figure 6d that functional groups such as carboxyl, carbonyl and olefin were added, which are aligned with the functional groups carried by PHA in Figure 4, which again verified that PHA was successfully loaded onto BC. XPS analysis of BC and PHABC before and after adsorption was performed (Figure 6e). After Pb^{2+} adsorption, binding energy at about 140

https://doi.org/10.1021/acsomega.2c08192
ACS Omega 2023, 8, 12206−12216

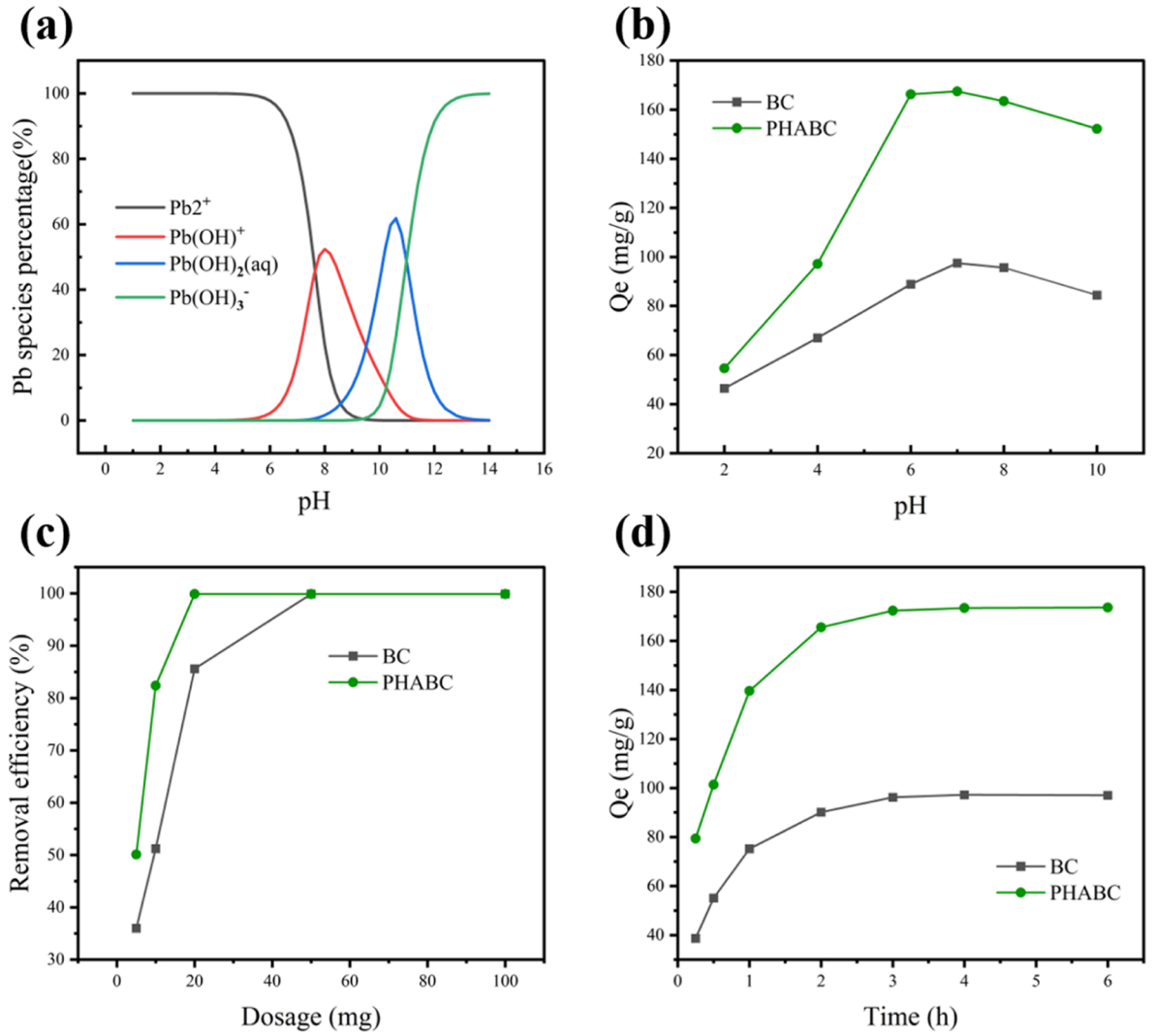

Figure 7. (a) Pb^{2+} speciation predicted by Visual MINTEQ (version 3.1), Pb = 50 mg/L; effects of (b) solution pH, (c) adsorbent dosage, and (d) contact time on the adsorption capacities of BC and PHABC (volume = 40 mL and T = 298 K).

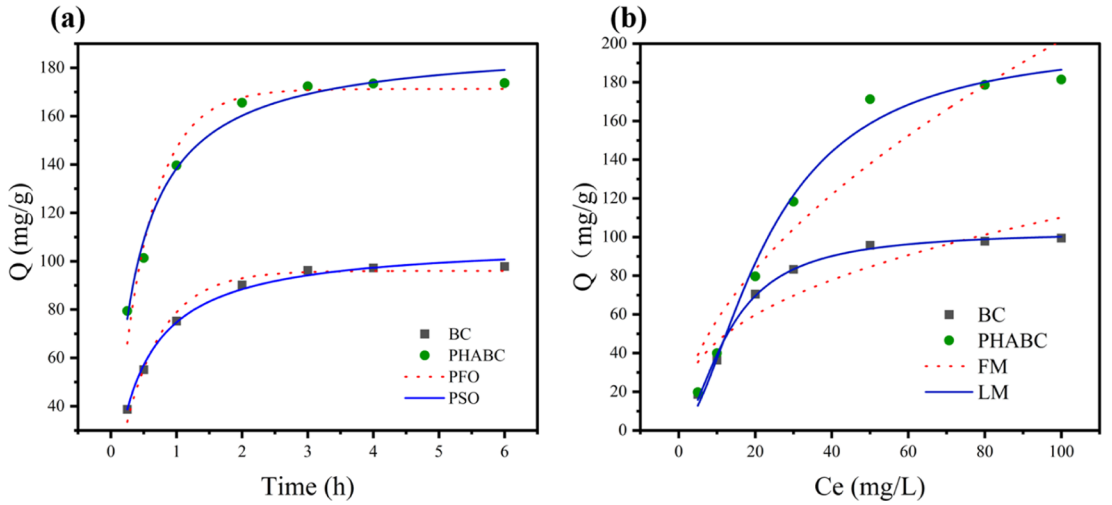

Figure 8. (a) Nonlinear PFO and PSO kinetic models and (b) LM and FM models (dosage = 10 mg, volume = 40 mL, initial Pb^{2+} concentration = 50 mg/L, pH = 7, and T = 298 K).

eV was observed on the biochar, which corresponds to the characteristic peak of Pb^{2+}, indicating that Pb^{2+} was successfully adsorbed by the biochar. Figure 6f shows even more clearly that the adsorption capacity of PHABC for Pb^{2+} is greatly enhanced.

https://doi.org/10.1021/acsomega.2c08192
ACS Omega 2023, 8, 12206−12216

Table 6. Adsorption Kinetic

	kinetic model									
	PFO					PSO				
samples	q_e (mg/g)	SE	K_1 (h^{-1})	SE	R^2	q_e (mg/g)	SE	K_2 (g/mg/h)	SE	R^2
BC	96.01	1.738	1.720	0.124	0.981	108.26	1.645	2.223	0.148	0.993
PHABC	171.25	3.862	1.946	0.181	0.963	190.33	4.010	2.659	0.262	0.982

Table 7. Isothermal Model

	isothermal model									
	LM					FM				
samples	q_m (mg/g)	SE	K_L (L/mg)	SE	R^2	K_F (mg/g) $(mg/L)^{-n}$	SE	$1/n$	SE	R^2
BC	103.03	2.273	0.011	0.003	0.995	19.10	6.659	0.380	0.087	0.823
PHABC	201.71	14.069	0.004	0.003	0.984	16.11	6.752	0.549	0.101	0.895

3.3.2. Adsorption Experiment. Based on Visual MINTEQ software, the distribution of Pb^{2+} species was determined at pH 1−14 (Figure 7a). Pb^{2+} was the dominant species at pH 1.0−7.0, while $Pb(OH)_2(aq)$ was dominant at pH 8.0−12.0. These results are consistent with the observation of Pb^{2+} precipitation when pH > 8.0. To determine the adsorption mechanism and the suitable adsorption range of the biochar materials, the adsorption capacity of BC and PHABC was examined in the pH range of 2−10. From Figure 7b, it can be seen that pH had a great effect on the adsorption capacity of biochar, and adsorption capacity increased significantly with the increased initial pH of the solution, reaching the optimum at pH = 7. Under our subsequent experimental conditions, elemental Pb exists mainly as Pb^{2+} and contains a small amount of $Pb(OH)^+$. Biochar can effectively adsorb both ions. And the total amount of elemental Pb was 50 mg/L at maximum, which could ensure that it existed in the solution in ionic form instead of generating a precipitate. A comparison was made of the removal effect in the range of 5−100 mg for 40 mL 50 mg·L^{-1}. As demonstrated in Figure 7c, the removal of BC and PHABC increased from 36.7 and 50.1% to 51.5 and 82.4%, respectively, when the adsorbent dosage was increased from 5 to 10 mg. It is due to the increase in adsorbent dosage, adsorbent surface area, and adsorption sites favorable for the contact between Pb^{2+} and biochar. Moreover, the removal rate of PHA reached up to 99.9% when the adsorbent amount was increased from 10 to 20 mg, indicating the absorption of almost all Pb^{2+} in the solution at this time. To investigate the adsorption capacity of PHABC, a dosage of 10 mg was more suitable. The contact time during adsorption experiments also has an effect on the adsorption capacity, as shown in Figure 8d, and the adsorption amount rises sharply within 1 h and tends to equilibrium after 2 h. Hence, pH = 7 and 10 mg dosing amount were selected for subsequent adsorption experiments considerating the removal efficiency and economic benefits.

3.3.3. Adsorption Kinetic and Isothermal Model. The results of BC and PHABC fitted Pb^{2+} adsorption kinetics are presented in Table 6. Based on the R-square (R^2) and standard error (SE), it can be seen that the secondary kinetic model was more suitable for Pb^{2+} adsorption kinetics, which indicated that the chemisorption process can be used as a rate-limiting step one.(Table 7) The adsorption rate of biochar samples is more likely to be controlled by multiple mechanisms (e.g., due to surface coordination and precipitation of functional components). In most previous studies, the kinetics of Pb^{2+} adsorption on biochar were well described by PSO models.[53−55] The maximum removal rate of 190.33 mg·g^{-1} for the secondary kinetic model was better than that of similar adsorbent materials. The adsorption capacity of Pb^{2+} in this study is greater than that of other adsorbents (Table 8). The FM and LM isothermal models (Figure 8b) were used for describing the association between the equilibrium adsorption capacities of BC and PHABC on Pb^{2+} and the equilibrium concentration of Pb in the solution. By this means, insight was gained into the adsorption process and the mechanism of Pb ions by the BC at a constant temperature. Like kinetics, the adsorption of Pb^{2+} underwent a similar initial fast ratio followed by a slow period. Compared to the FM in Figure 8b, the experimental data are more consistent with the LM model, indicating that Pb^{2+} adsorption can be considered as a monolayer reaction.

Table 8. Comparison of Different Adsorbents Used for Pb^{2+} Removal

adsorbents	pH	Q_{max} (mg/g)	references
HA-modified pine cone biochar	7.0	190.24	this work
coconut fiber biochar	6.0	47.92	44
magnetic date biochar	5.5	103.09	45
H_2O_2-modified watermelon seeds biochar	5.0	60.87	46
peanut shell biochar	5.0	11.05	47
modified hickory wood biochar	6.0	153.11	48
$KMnO_4$-modified biochar	5.0	37.51	49
magnetic corn straw biochar	5.5	93.24	50
iron-coated empty fruit string biochar		142.86	51
magnetic magnetite nanoparticles	5.0	53.11	52

4. CONCLUSIONS

In this paper, a simple and effective method was proposed to extract HAs with higher purity and lower ash content from lignite after HNO_3 pretreatment under alkaline hydrothermal conditions. The adsorption behavior of the extracted HA-activated biochar on lead ions was also studied, and the following conclusions were reached:

(1) The changes in inorganic elements and functional groups during acid and hydrothermal treatments were investigated using SEM-EDS, FTIR, XRD, ICP−OES, and other analytical techniques. Acid treatment removed the ash and mineral components of lignite and introduced numerous oxygen-containing polar functional groups, like carboxyl and carbonyl groups. The hydrothermal treatment effectively increased HA yield, and the combination

https://doi.org/10.1021/acsomega.2c08192
ACS Omega 2023, 8, 12206−12216

of acid pretreatment and hydrothermal treatment effectively reduced heavy metal ions in HAs.

(2) PHA was used as an activator of biochar to improve its adsorption performance. The results showed that the pore volume and pore size of BC experienced an increase after activation. FTIR also indicated that functional groups, such as carboxyl, carbonyl, and olefin groups, increased in biochar after loading PHA.

(3) The PHA-modified biochar was subjected to Pb^{2+} adsorption experiments, and an adsorption capacity of 173.6 $mg \cdot g^{-1}$ was obtained at pH = 7, a dosage of 10 mg, and an optimal temperature of 25 °C. The adsorption process was in accordance with the secondary kinetic model and Langmuir model.

AUTHOR INFORMATION

Corresponding Author

Jie Yuan − *School of Chemistry and Materials Engineering, Liupanshui Normal University, Liupanshui 553004 Guizhou, China*; orcid.org/0000-0002-8166-6132; Email: yuanjieedu@163.com

Authors

Huijin Li − *College of Environmental and Chemical Engineering, Dalian University, Dalian 116622 Liaoning, China*

Shuang Ding − *College of Environmental and Chemical Engineering, Dalian University, Dalian 116622 Liaoning, China*

Complete contact information is available at: https://pubs.acs.org/10.1021/acsomega.2c08192

Notes

The authors declare no competing financial interest.

ACKNOWLEDGMENTS

This study is supported by the National Natural Science Foundation of China (51904150), the Guizhou Province Ordinary Universities Scientific Talents Project (KY[2019] 056), the Liupanshui Science and Technology Plan Project (52020-2022-PT-04), and the Liu Panshui Normal University Scientific Research and Cultivation Projects (LPSSYL-PY202127).

REFERENCES

(1) de Melo, B. A. G.; Motta, F. L.; Santana, M. H. A. Humic Acids: Structural Properties and Multiple Functionalities for Novel Technological Developments. *Mater. Sci. Eng. C* **2016**, *62*, 967−974.

(2) de Souza, F.; Bragança, S. R. Extraction and Characterization of Humic Acid from Coal for the Application as Dispersant of Ceramic Powders. *J. Mater. Res. Technol.* **2018**, *7*, 254−260.

(3) Yang, F.; Antonietti, M. The Sleeping Giant: A Polymer View on Humic Matter in Synthesis and Applications. *Prog. Polym. Sci.* **2020**, *100*, 101182.

(4) Chianese, S.; Fenti, A.; Iovino, P.; Musmarra, D.; Salvestrini, S. Sorption of Organic Pollutants by Humic Acids: A Review. *Molecules* **2020**, *25*, 918.

(5) Klavins, M.; Eglite, L.; Serzane, J. Methods for Analysis of Aquatic Humic Substances. *Crit. Rev. Anal. Chem.* **1999**, *29*, 187−193.

(6) Colella, A.; de Gennaro, B.; Salvestrini, S.; Colella, C. Surface Interaction of Humic Acids with Natural and Synthetic Phillipsite. *J. Porous Mater.* **2015**, *22*, 501−509.

(7) Pomeroy, B.; Grilc, M.; Gyergyek, S.; Likozar, B. Catalyst Structure-Based Hydroxymethylfurfural (HMF) Hydrogenation Mechanisms, Activity and Selectivity over Ni. *Chem. Eng. J.* **2021**, *412*, 127553.

(8) Slak, J.; Pomeroy, B.; Kostyniuk, A.; Grilc, M.; Likozar, B. A Review of Bio-Refining Process Intensification in Catalytic Conversion Reactions, Separations and Purifications of Hydroxymethylfurfural (HMF) and Furfural. *Chem. Eng. J.* **2022**, *429*, 132325.

(9) Šivec, R.; Grilc, M.; Huš, M.; Likozar, B. Multiscale Modeling of (Hemi)Cellulose Hydrolysis and Cascade Hydrotreatment of 5-Hydroxymethylfurfural, Furfural, and Levulinic Acid. *Ind. Eng. Chem. Res.* **2019**, *58*, 16018−16032.

(10) Klučáková, M.; Pavlíková, M. Lignitic Humic Acids as Environmentally-Friendly Adsorbent for Heavy Metals. *J. Chem-ny.* **2017**, *2017*, 1−5.

(11) Zara, M.; Ahmad, Z.; Akhtar, J.; Shahzad, K.; Sheikh, N.; Munir, S. Extraction and Characterization of Humic Acid from Pakistani Lignite Coals. *Energy Sources, Part A* **2017**, *39*, 1159−1166.

(12) Stefanova, M.; Gonsalvesh, L.; Marinov, S.; Czech, J.; Carleer, R.; Yperman, J. Reductive Pyrolysis of Miocene-Aged Lignite Humic Acids, Bulgaria. *Fuel* **2016**, *165*, 324−330.

(13) Tahmasebi, A.; Yu, J.; Li, X.; Meesri, C. Experimental Study on Microwave Drying of Chinese and Indonesian Low-Rank Coals. *Fuel Process. Technol.* **2011**, *92*, 1821−1829.

(14) Burange, A. S.; Ahmad, A.; Luque, R. Electrophilicity in Heterogeneous Catalysis: Role of Surface and Sub-Surface Modification. *Catal. Sci. Technol.* **2021**, *11*, 4315−4326.

(15) Öztaş, N. A.; Yürüm, Y. Pyrolysis of Turkish Zonguldak Bituminous Coal. Part 1. Effect of Mineral Matter. *Fuel* **2000**, *79*, 1221−1227.

(16) Hiradate, S.; Yonezawa, T.; Takesako, H. Isolation and Purification of Hydrophilic Fulvic Acids by Precipitation. *Geoderma* **2006**, *132*, 196−205.

(17) Li, X. H.; Li, H. J.; Wang, R. Q.; Feng, J.; Li, W. Y. Acid Pretreatment Effect on Oxygen Migration during Lignite Pyrolysis. *Fuel* **2020**, *262*, 116650.

(18) Jaiswal, Y.; Pal, S. L.; Jaiswal, H.; Jain, A.; Kush, L.; Rai, D.; Tatar, D. An Investigation of Changes in Structural Parameters and Organic Functional Groups of Inertinite Rich Lignite during Acid Treatment Processes. *Energy Sources, Part A* **2021**, 1−18.

(19) Huang, B.; Liu, G.; Wang, P.; Zhao, X.; Xu, H. Effect of Nitric Acid Modification on Characteristics and Adsorption Properties of Lignite. *Processes* **2019**, *7*, 167.

(20) Li, G.-Y.; Ding, J.-X.; Zhang, H.; Hou, C.-X.; Wang, F.; Li, Y.-Y.; Liang, Y.-H. ReaxFF Simulations of Hydrothermal Treatment of Lignite and Its Impact on Chemical Structures. *Fuel* **2015**, *154*, 243−251.

(21) Sriramoju, S. K.; Babu, V.; Dash, P. S.; Majumdar, S.; Shee, D. Effective Utilization of Coal Processing Waste: Separation of Low Ash Clean Coal from Washery Rejects by Hydrothermal Treatment. *Miner. Process. Extr. Metall.* **2022**, *43*, 165−181.

(22) Liu, J.; Wu, J.; Zhu, J.; Wang, Z.; Zhou, J.; Cen, K. Removal of Oxygen Functional Groups in Lignite by Hydrothermal Dewatering: An Experimental and DFT Study. *Fuel* **2016**, *178*, 85−92.

(23) Tang, W.-W.; Zeng, G.-M.; Gong, J.-L.; Liang, J.; Xu, P.; Zhang, C.; Huang, B.-B. Impact of Humic/Fulvic Acid on the Removal of Heavy Metals from Aqueous Solutions Using Nanomaterials: A Review. *Sci. Total Environ.* **2014**, *468−469*, 1014−1027.

(24) Zhao, J.; Liang, G.; Zhang, X.; Cai, X.; Li, R.; Xie, X.; Wang, Z. Coating Magnetic Biochar with Humic Acid for High Efficient Removal of Fluoroquinolone Antibiotics in Water. *Sci. Total Environ.* **2019**, *688*, 1205−1215.

(25) Zhang, M.; Shu, L.; Guo, X.; Shen, X.; Zhang, H.; Shen, G.; Wang, B.; Yang, Y.; Tao, S.; Wang, X. Impact of Humic Acid Coating on Sorption of Naphthalene by Biochars. *Carbon* **2015**, *94*, 946−954.

(26) Yang, F.; Du, Q.; Sui, L.; Cheng, K. One-Step Fabrication of Artificial Humic Acid-Functionalized Colloid-like Magnetic Biochar for Rapid Heavy Metal Removal. *Bioresour. Technol.* **2021**, *328*, 124825.

(27) Guo, J.; Yan, C.; Luo, Z.; Fang, H.; Hu, S.; Cao, Y. Synthesis of a Novel Ternary HA/Fe-Mn Oxides-Loaded Biochar Composite and Its

Application in Cadmium(II) and Arsenic(V) Adsorption. *J. Environ. Sci.* **2019**, *85*, 168−176.
(28) Ahmad, M.; Rajapaksha, A. U.; Lim, J. E.; Zhang, M.; Bolan, N.; Mohan, D.; Vithanage, M.; Lee, S. S.; Ok, Y. S. Biochar as a Sorbent for Contaminant Management in Soil and Water: A Review. *Chemosphere* **2014**, *99*, 19−33.
(29) Wang, J.; Wang, S. Preparation, Modification and Environmental Application of Biochar: A Review. *J. Cleaner Prod.* **2019**, *227*, 1002−1022.
(30) Proximate Analysis of Coal; GB/T212-2008; *The State Standard of the People's Republic of China*; Standards Press of China: Beijing, 2009.
(31) Du, Q.; Li, G.; Zhang, S.; Song, J.; zhao, Y.; Yang, F. High-Dispersion Zero-Valent Iron Particles Stabilized by Artificial Humic Acid for Lead Ion Removal. *J. Hazard. Mater.* **2020**, *383*, 121170.
(32) Wang, Y.; Mei, F.; Xue, S. Comparative Analysis of Microstructure Evolution and Oxidation Performance of Acid-Treated Lignite. *Fuel Process. Technol.* **2021**, *215*, 106750.
(33) Sabar, M. A.; Ali, M. I.; Fatima, N.; Malik, A. Y.; Jamal, A.; Liaquat, R.; He, H.; Liu, F.-J.; Guo, H.; Urynowicz, M.; Huang, Z. Evaluation of Humic Acids Produced from Pakistani Subbituminous Coal by Chemical and Fungal Treatments. *Fuel* **2020**, *278*, 118301.
(34) Fatima, N.; Jamal, A.; Huang, Z.; Liaquat, R.; Ahmad, B.; Haider, R.; Ali, M. I.; Shoukat, T.; ALOthman, Z. A.; Ouladsmane, M.; Ali, T.; Ali, S.; Akhtar, N.; Sillanpää, M. Extraction and Chemical Characterization of Humic Acid from Nitric Acid Treated Lignite and Bituminous Coal Samples. *Sustainability* **2021**, *13*, 8969.
(35) Xu, M.; Guo, F.; Zhang, Y.; Yang, Z.; Cao, Y.; Gui, X.; Xing, Y. Effect of Hydrothermal Pretreatment on Surface Physicochemical Properties of Lignite and Its Flotation Response. *Powder Technol.* **2021**, *386*, 81−89.
(36) Gómez-Serrano, V.; Fernández-González, M. C.; Cuerda-Correa, E. M.; Macías-García, A.; Alexandre-Franco, M. F.; Rojas-Cervantes, M. L. Physico-Chemical Properties of Low-Rank Coals. *Powder Technol.* **2004**, *148*, 38−42.
(37) Ye, C.-P.; Yang, Z.-J.; Li, W.-Y.; Rong, H.-L.; Feng, J. Effect of Adjusting Coal Properties on HulunBuir Lignite Pyrolysis. *Fuel Process. Technol.* **2017**, *156*, 415−420.
(38) Shi, Z.; Jin, L.; Zhou, Y.; Li, Y.; Hu, H. Effect of Hydrothermal Treatment on Structure and Liquefaction Behavior of Baiyinhua Coal. *Fuel Process. Technol.* **2017**, *167*, 648−654.
(39) Javaid, R.; Qazi, U. Y.; Ikhlaq, A.; Zahid, M.; Alazmi, A. Subcritical and Supercritical Water Oxidation for Dye Decomposition. *J. Environ. Manage.* **2021**, *290*, 112605.
(40) Cheng, Y.; Xue, F.; Yu, S.; Du, S.; Yang, Y. Subcritical Water Extraction of Natural Products. *Molecules* **2021**, *26*, 4004.
(41) Kurková, M.; Klika, Z.; Kliková, C.; Havel, J. Humic Acids from Oxidized Coals. *Chemosphere* **2004**, *54*, 1237−1245.
(42) Li, H.; Ye, X.; Geng, Z.; Zhou, H.; Guo, X.; Zhang, Y.; Zhao, H.; Wang, G. The Influence of Biochar Type on Long-Term Stabilization for Cd and Cu in Contaminated Paddy Soils. *J. Hazard. Mater.* **2016**, *304*, 40−48.
(43) Imran, M.; Khan, Z. U. H.; Iqbal, M. M.; Iqbal, J.; Shah, N. S.; Munawar, S.; Ali, S.; Murtaza, B.; Naeem, M. A.; Rizwan, M. Effect of Biochar Modified with Magnetite Nanoparticles and HNO_3 for Efficient Removal of Cr(VI) from Contaminated Water: A Batch and Column Scale Study. *Environ. Pollut.* **2020**, *261*, 114231.
(44) Wu, F.; Pu, N.; Ye, G.; Sun, T.; Wang, Z.; Song, Y.; Wang, W.; Huo, X.; Lu, Y.; Chen, J. Performance and Mechanism of Uranium Adsorption from Seawater to Poly(Dopamine)-Inspired Sorbents. *Environ. Sci. Technol.* **2017**, *51*, 4606−4614.
(45) Zahedifar, M.; Seyedi, N.; Shafiei, S.; Basij, M. Surface-Modified Magnetic Biochar: Highly Efficient Adsorbents for Removal of Pb(II) and Cd(II). *Mater. Chem. Phys.* **2021**, *271*, 124860.
(46) Ahmed, W.; Mehmood, S.; Núñez-Delgado, A.; Ali, S.; Qaswar, M.; Shakoor, A.; Mahmood, M.; Chen, D.-Y. Enhanced Adsorption of Aqueous Pb(II) by Modified Biochar Produced through Pyrolysis of Watermelon Seeds. *Sci. Total Environ.* **2021**, *784*, 147136.
(47) Lee, M.-E.; Park, J. H.; Chung, J. W. Comparison of the Lead and Copper Adsorption Capacities of Plant Source Materials and Their Biochars. *J. Environ. Manage.* **2019**, *236*, 118−124.
(48) Wang, H.; Gao, B.; Wang, S.; Fang, J.; Xue, Y.; Yang, K. Removal of Pb(II), Cu(II), and Cd(II) from Aqueous Solutions by Biochar Derived from $KMnO_4$ Treated Hickory Wood. *Bioresour. Technol.* **2015**, *197*, 356−362.
(49) El-Banna, M. F.; Mosa, A.; Gao, B.; Yin, X.; Ahmad, Z.; Wang, H. Sorption of Lead Ions onto Oxidized Bagasse-Biochar Mitigates Pb-Induced Oxidative Stress on Hydroponically Grown Chicory: Experimental Observations and Mechanisms. *Chemosphere* **2018**, *208*, 887−898.
(50) Cao, B.; Qu, J.; Yuan, Y.; Zhang, W.; Miao, X.; Zhang, X.; Xu, Y.; Han, T.; Song, H.; Ma, S.; Tian, X.; Zhang, Y. Efficient Scavenging of Aqueous Pb(II)/Cd(II) by Sulfide-Iron Decorated Biochar: Performance, Mechanisms and Reusability Exploration. *J. Environ. Chem. Eng.* **2022**, *10*, 107531.
(51) Fahmi, A. H.; Samsuri, A. W.; Singh, D. Magnetization Improved Fine Particle Biochar Adsorption of Lead. *Soil Sediment Contam.* **2022**, *31*, 633−654.
(52) Rajput, S.; Pittman, C. U.; Mohan, D. Magnetic Magnetite (Fe_3O_4) Nanoparticle Synthesis and Applications for Lead (Pb^{2+}) and Chromium (Cr^{6+}) Removal from Water. *J. Colloid Interface Sci.* **2016**, *468*, 334−346.
(53) Liang, J.; Li, X.; Yu, Z.; Zeng, G.; Luo, Y.; Jiang, L.; Yang, Z.; Qian, Y.; Wu, H. Amorphous MnO2 Modified Biochar Derived from Aerobically Composted Swine Manure for Adsorption of Pb (II) and Cd (II). *ACS Sustainable Chem. Eng.* **2017**, *5*, 5049.
(54) Yang, W.; Liu, Y.; Pan, J. Experimental and Kinetic Study on Hg0 Removal by Microwave/Hydrogen Peroxide Modified Seaweed-Based Porous Biochars. *Environ. Technol. Innovation* **2021**, *22*, 101411.
(55) Fan, Z.; Fang, J.; Zhang, G.; Qin, L.; Fang, Z.; Jin, L. Improved Adsorption of Tetracycline in Water by a Modified Caulis Spatholobi Residue Biochar. *ACS Omega* **2022**, *7*, 30543−30553.

https://doi.org/10.1021/acsomega.2c08192
ACS Omega 2023, 8, 12206−12216